

Forces of a single-beam gradient laser trap on a dielectric sphere in the ray optics regime

A. Ashkin

AT&T Bell Laboratories, Holmdel, New Jersey 07733

ABSTRACT We calculate the forces of single-beam gradient radiation pressure laser traps, also called "optical tweezers," on micron-sized dielectric spheres in the ray optics regime. This serves as a simple model system for describing laser trapping and manipulation of living cells and organelles within cells. The gradient and scattering forces are defined for beams of complex shape in the ray-optics limit. Forces are calculated over the entire cross-section of the sphere using TEM_{00} and TEM_{01}^* mode input intensity profiles and spheres of varying index of refraction. Strong uniform traps are possible with force variations less than a factor of 2 over the sphere cross-section. For a laser power of 10 mW and a relative index of refraction of 1.2 we compute trapping forces as high as $\sim 1.2 \times 10^{-6}$ dynes in the weakest (backward) direction of the gradient trap. It is shown that good trapping requires high convergence beams from a high numerical aperture objective. A comparison is given of traps made using bright field or differential interference contrast optics and phase contrast optics.

INTRODUCTION

This paper gives a detailed description of the trapping of micron-sized dielectric spheres by a so-called single-beam gradient optical trap. Such dielectric spheres can serve as first simple models of living cells in biological trapping experiments and also as basic particles in physical trapping experiments. Optical trapping of small particles by the forces of laser radiation pressure has been used for about 20 years in the physical sciences for the manipulation and study of micron and submicron dielectric particles and even individual atoms (1-7). These techniques have also been extended more recently to biological particles (8-18).

The basic forces of radiation pressure acting on dielectric particles and atoms are known (1, 2, 19-21). For dielectric spheres large compared with the wavelength, one is in the geometric optics regime and can thus use simple ray optics in the derivation of the radiation pressure force from the scattering of incident light momentum. This approach was used to calculate the forces for the original trapping experiments on micron-sized dielectric spheres (1, 22). These early traps were either all optical two-beam traps (1) or single beam levitation traps which required gravity or electrostatic forces for their stability (23, 24). For particles in the Rayleigh regime where the size is much less than the wavelength λ the particle acts as a simple dipole. The force on a dipole divides itself naturally into two components: a so-called scattering force component pointing in the direction of the incident light and a gradient component pointing in the direction of the intensity gradient of the light (19, 21).

The single-beam gradient trap, sometimes referred to as "optical tweezers," was originally designed for Rayleigh particles (20). It consists of a single strongly focused laser beam. Conceptually and practically it is one of the simplest laser traps. Its stability in the Rayleigh regime is the result of the dominance of the gradient force pulling particles toward the high focus of the beam over the scattering force trying to push particles away from the focus in the direction of the incident light. Subsequently it was found experimentally that single-beam gradient traps could also trap and manipulate micron-sized (25) and a variety of biological particles, including living cells and organelles within living cells (8, 10). Best results were obtained using infrared trapping beams to reduced optical damage. The trap in these biological applications was built into a standard high resolution microscope in which one uses the same high numerical aperture (NA) microscope objective for both trapping and viewing. The micromanipulative abilities of single-beam gradient traps are finding use in a variety of experiments in the biological sciences. Experiments have been performed in the trapping of viruses and bacteria (8); the manipulation of yeast cells, blood cells, protozoa, and various algae and plant cells (10); the measurement of the compliance of bacterial flagella (11); internal cell surgery (13); manipulation of chromosomes (12); trapping and force measurement on sperm cells (14, 15); and recently, observations on the force of motor molecules driving mitochondrion and latex spheres along microtubules (16, 17). Optical techniques have also been used for cell sorting (9).

Qualitative descriptions of the operation of the single-beam gradient trap in the ray optics regime have already been given (25, 26). In Fig. 1 taken from reference 26, the action of the trap on a dielectric sphere is described in terms of the total force due to a typical pair of rays a and b of the converging beam, under the simplifying assumption of zero surface reflection. In this approximation the forces F_a and F_b are entirely due to refraction and are shown pointing in the direction of the momentum change. One sees that for arbitrary displacements of the sphere origin O from the focus f that the vector sum of F_a and F_b gives a net restoring force F directed back to the focus, and the trap is stable. In this paper we quantify the above qualitative picture of the trap. We show how to define the gradient and scattering force on a sphere $\gg \lambda$ in a natural way for beams of arbitrary shape. One can then describe trapping in the ray optics regime in the same terms as in the Rayleigh regime.

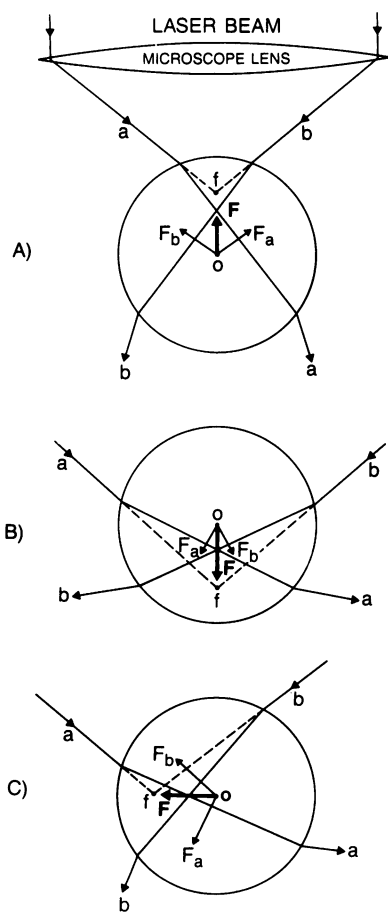


FIGURE 1 Qualitative view of the trapping of dielectric spheres. The refraction of a typical pair of rays a and b of the trapping beam gives forces F_a and F_b , whose vector sum F is always restoring for axial and transverse displacements of the sphere from the trap focus f .

Results are given for the trapping forces over the entire cross-section of the sphere. The forces are calculated for input beams with various TEM_{00} and TEM_{01}^* mode intensity profiles at the input aperture of a high numerical aperture trapping objective of $NA = 1.25$. The results confirm the qualitative observation that good trapping requires the input aperture to be well enough filled by the incident beam to give rise to a trapping beam with high convergence angle. One can design traps in which the trapping forces vary at most by a factor of ~ 1.8 over the cross-section of the sphere with trapping forces as high as $Q = 0.30$ where the force F is given in terms of the dimensionless factor Q in the expression $F = Q(n_1 P/c)$. P is the incident power and $n_1 P/c$ is the incident momentum per second in a medium of index of refraction n_1 . There has been a previous calculation of single-beam gradient trapping forces on spheres in the geometrical optics limit by Wright et al. (27), over a limited portion of the sphere, which gives much poorer results. They find trapping forces of $Q = 0.055$ in the above units which vary over the sphere cross-section by more than an order of magnitude.

LIGHT FORCES IN THE RAY OPTICS REGIME

In the ray optics or geometrical optics regime one decomposes the total light beam into individual rays, each with appropriate intensity, direction, and state of polarization, which propagate in straight lines in media of uniform refractive index. Each ray has the characteristics of a plane wave of zero wavelength which can change directions when it reflects, refracts, and changes polarization at dielectric interfaces according to the usual Fresnel formulas. In this regime diffractive effects are neglected (see Chapter III of reference 28).

The simple ray optics model of the single-beam gradient trap used here for calculating the trapping forces on a sphere of diameter $\gg \lambda$ is illustrated in Fig. 2. The trap consists of an incident parallel beam of arbitrary mode structure and polarization which enters a high NA microscope objective and is focused ray-by-ray to a dimensionless focal point f . Fig. 2 shows the case where f is located along the Z axis of the sphere. The maximum convergence angle for rays at the edge of the input aperture of a high NA objective lens such as the Leitz PL APO 1.25W (E. Leitz, Inc., Wetzlar, Germany) or the Zeiss PLAN NEOFLUAR 63/1.2W water immersion objectives (Carl Zeiss, Inc., Thornwood, NY), for example, is $\phi_{max} \approx 70^\circ$. Computation of the total force on the sphere consists of summing the contributions of each beam ray entering the aperture at radius r with respect to the beam axis and angle β with respect the Y axis. The effect of neglecting the finite size of the actual beam focus, which can approach the limit of $\lambda/2n_1$ (see reference 29), is negligible for spheres much larger than λ . The point focus description of the convergent beam in which the ray directions and momentum continue in straight lines through the focus gives the correct incident polarization and momentum for each ray. The rays then reflect and refract at the surface of the sphere giving rise to the light forces.

The model of Wright et al. (27) tries to describe the single-beam gradient trap in terms of both wave and ray optics. It uses the TEM_{00} Gaussian mode beam propagation formula to describe the focused trapping beam and takes the ray directions of the individual rays to be

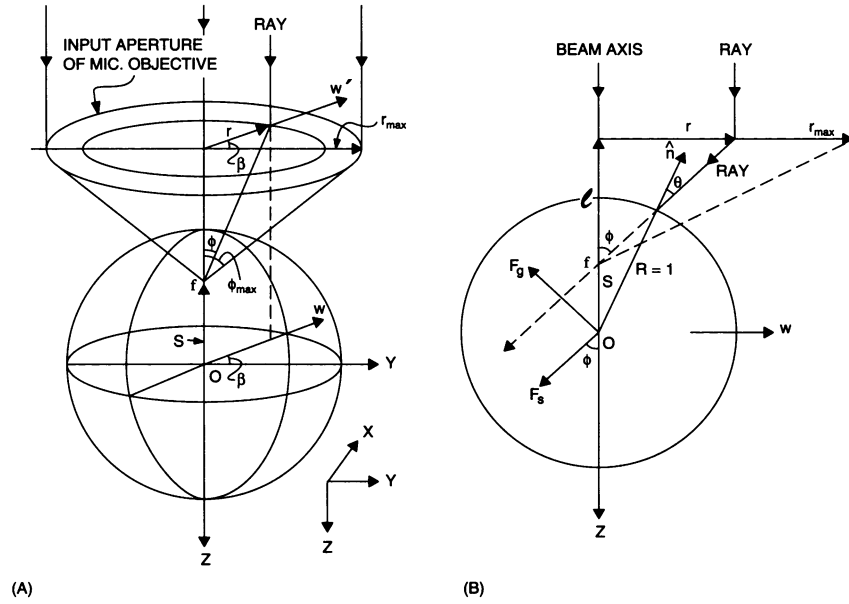


FIGURE 2 (A) Single beam gradient force trap in the ray optics model with beam focus f located along the Z axis of the sphere. (B) Geometry of an incident ray giving rise to gradient and scattering force contributions F_g and F_s .

perpendicular to the Gaussian beam phase fronts. Since the curvature of the phase fronts vary considerably along the beam, the ray directions also change, from values as high as 30° or more with respect to the beam axis in the far-field, to 0° at the beam focus. This is physically incorrect. It implies that rays can change their direction in a uniform medium, which is contrary to geometrical optics. It also implies that the momentum of the beam can change in a uniform medium without interacting with a material object, which violates the conservation of light momentum. The constancy of the light momentum and ray direction for a Gaussian beam can be seen in another way. If one resolves a Gaussian beam into an equivalent angular distribution of plane waves (see Section 11.4.2 of reference 28) one sees that these plane waves can propagate with no momentum or direction changes right through the focus. Another important point is that the Gaussian beam propagation formula is strictly correct only for transversely polarized beams in the limit of small far-field diffraction angles θ' , where $\theta' = \lambda/\pi w_0$ (w_0 being the focal spot radius). This formula therefore provides a poor description of the high convergence beams used in good traps. The proper wave description of a highly convergent beam is much more complex than the Gaussian beam formula. It involves strong axial electric field components at the focus (from the edge rays) and requires use of the vector wave equation as opposed to the scalar wave equation used for Gaussian beams (30).

Apart from the major differences near the focus, the model of Wright et al. (27) should be fairly close to the ray optics model used here in the far-field of the trapping beam. The principal distinction between the two calculations, however, is the use by Wright et al. of beams with relatively small convergence angle. They calculate forces for beams with spot sizes $w_0 = 0.5, 0.6,$ and $0.7 \mu\text{m}$, which implies values of θ' of $\sim 29, 24,$ and 21° , respectively. Therefore, these are beams having relatively small convergence angles compared with convergence angles of $\phi_{\text{max}} \cong 70^\circ$ which are available from a high NA objective.

Consider first the force due to a single ray of power P hitting a dielectric sphere at an angle of incidence θ with incident momentum

per second of $n_1 P/c$ (see Fig. 3). The total force on the sphere is the sum of contributions due to the reflected ray of power PR and the infinite number of emergent refracted rays of successively decreasing power $PT^2, PT^2R, \dots, PT^{2n}, \dots$. The quantities R and T are the Fresnel reflection and transmission coefficients of the surface at θ . The net force acting through the origin O can be broken into F_z and F_y components as given by Roosen and co-workers (3, 22) (see Appendix I for a sketch of the derivation).

$$F_z = F_s = \frac{n_1 P}{c} \left\{ 1 + R \cos 2\theta - \frac{T^2 [\cos(2\theta - 2r) + R \cos 2\theta]}{1 + R^2 + 2R \cos 2r} \right\} \quad (1)$$

$$F_y = F_g = \frac{n_1 P}{c} \left\{ R \sin 2\theta - \frac{T^2 [\sin(2\theta - 2r) + R \sin 2\theta]}{1 + R^2 + 2R \cos 2r} \right\} \quad (2)$$

where θ and r are the angles of incidence and refraction. These formulas sum over all scattered rays and are therefore exact. The forces are polarization dependent since R and T are different for rays polarized perpendicular or parallel to the plane of incidence.

In Eq. 1 we denote the F_z component pointing in the direction of the incident ray as the scattering force component F_s for this single ray. Similarly, in Eq. 2 we denote the F_y component pointing in the direction perpendicular to the ray as the gradient force component F_g for the ray. For beams of complex shape such as the highly convergent beams used in the single-beam gradient trap, we define the scattering and gradient forces of the beam as the vector sums of the scattering and gradient force contributions of the individual rays of the beam. Fig. 2B depicts the direction of the scattering force component and gradient force component of a single ray of the convergent beam

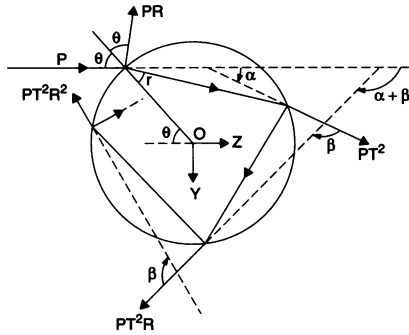


FIGURE 3 Geometry for calculating the force due to the scattering of a single incident ray of power P by a dielectric sphere, showing the reflected ray PR and infinite set of refracted rays PT^2R^n .

striking the sphere at angle θ . One can show that the gradient force as defined above is conservative. This follows from the fact that F_g , the gradient force for a ray, can be expressed solely as a function of ρ , the radial distance from the ray to the particle. This implies that the integral of the work done on a particle in going around an arbitrary closed path can be expressed as an integral of $F_g(\rho)d\rho$ which is clearly zero. If the gradient force for a single ray is conservative, then the gradient force for an arbitrary collection of rays is conservative. Thus the conservative property of the gradient force as defined in the geometrical optics regime is the same as in the Rayleigh regime. The work done by the scattering force, however, is always path dependent and is not conservative in any regime. As will be seen, these new definitions of gradient and scattering force for beams of more complex shape allow us to describe the operation of the gradient trap in the same manner in both the geometrical optics and Rayleigh regimes.

To get a feeling for the magnitudes of the forces, we calculate the scattering force F_s , the gradient force F_g , and the absolute magnitude of the total force $F_{mag} = (F_s^2 + F_g^2)^{1/2}$ as a function of the angle of incidence θ using Eqs. 1 and 2. We consider as a typical example the case of a circularly polarized ray hitting a sphere of effective index of refraction $n = 1.2$. The force for such a circularly polarized ray is the average of the forces for rays polarized perpendicular and parallel to the plane of incidence. The effective index of a particle is defined as the index of the particle n_2 divided by the index of the surrounding medium n_1 ; that is, $n = n_2/n_1$. A polystyrene sphere in water has $n = 1.6/1.33 \approx 1.2$. Fig. 4 shows the results for the forces F_s , F_g , and F_{mag} versus θ expressed in terms of the dimensionless factors Q_s , Q_g , and $Q_{mag} = (Q_s^2 + Q_g^2)^{1/2}$, where

$$F = Q \frac{n_1 P}{c}. \quad (3)$$

The quantity $n_1 P/c$ is the incident momentum per second of a ray of power P in a medium of index of refraction n_1 , (19, 31). Recall that the maximum radiation pressure force derivable from a ray of momentum per second $n_1 P/c$ corresponds to $Q = 2$ for the case of a ray reflected perpendicularly from a totally reflecting mirror. One sees that for $n = 1.2$ a maximum gradient force of Q_{gmax} as high as ~ 0.5 is generated for rays at angles of $\theta \approx 70^\circ$. Table I shows the effect of an index of refraction n on the maximum value of gradient force Q_{gmax} occurring at angle of incidence θ_{gmax} . The corresponding value of scattering force Q_s at θ_{gmax} is also listed. The fact that Q_s continues to grow relative to Q_{gmax} as n increases indicates potential difficulties in achieving good gradient traps at high n .

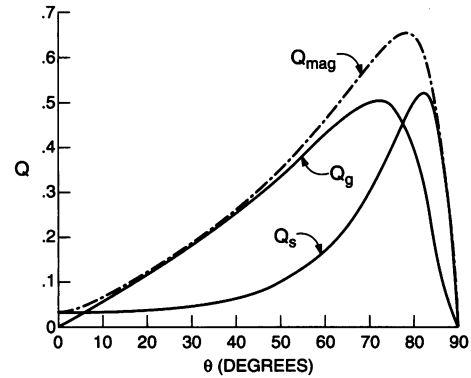


FIGURE 4 Values of the scattering force Q_s , gradient force Q_g , and magnitude of the total force Q_{mag} for a single ray hitting a dielectric sphere of index of refraction $n = 1.2$ at an angle θ .

FORCE OF THE GRADIENT TRAP ON SPHERES

Trap focus along Z axis

Consider the computation of the force of a gradient trap on a sphere when the focus f of the trapping beam is located along the Z axis at a distance S above the center of the sphere at O , as shown in Fig. 2. The total force on the sphere, for an axially-symmetric plane-polarized input trapping beam, is clearly independent of the direction of polarization by symmetry considerations. It can therefore be assumed for convenience that the input beam is circularly polarized with half the power in each of two orthogonally oriented polarization components. We find the force for a ray entering the input aperture of the microscope objective at an arbitrary radius r and angle β and then integrate numerically over the distribution of input rays using an AT&T 1600 PLUS personal computer. As seen in Fig. 2, the vertical plane ZW which is rotated by β from the ZY plane contains both the incident ray and the normal to the sphere \hat{n} . It is thus the plane of incidence. We can compute the angle of

TABLE 1 For a single ray. Effect of index of refraction n on maximum gradient force Q_{gmax} and scattering force Q_s occurring at angle of incidence θ_{gmax}

| n | Q_{gmax} | Q_s | θ_{gmax} |
|-----|------------|-------|-----------------|
| 1.1 | -0.429 | 0.262 | 79° |
| 1.2 | -0.506 | 0.341 | 72° |
| 1.4 | -0.566 | 0.448 | 64° |
| 1.6 | -0.570 | 0.535 | 60° |
| 1.8 | -0.547 | 0.625 | 59° |
| 2.0 | -0.510 | 0.698 | 59° |
| 2.5 | -0.405 | 0.837 | 64° |

incidence θ from the geometric relation $R \sin \theta = S \sin \phi$, where R is the radius of the sphere. We take $R = 1$ since the resultant forces in the geometric optics limit are independent of R . Knowing θ we can find F_g and F_s for the circularly polarized ray by first computing F_g and F_s for each of the two polarization components parallel and perpendicular to the plane of incidence using Eqs. 1 and 2 and adding the results. It is obvious by symmetry that the net force is axial. Thus for S above the origin O the contribution of each ray to the net force consists of a negative Z component $F_{gz} = -F_g \sin \phi$ and a positive Z component $F_{sz} = F_s \cos \phi$ as seen from Fig. 2B. For S below O the gradient force component changes sign and the scattering force component remains positive. We integrate out to a maximum radius r_{\max} for which $\phi = \phi_{\max} = 70^\circ$, the maximum convergence angle for a water immersion objective of NA = 1.25, for example. Consider first the case of a sphere of index of refraction $n = 1.2$ and an input beam which uniformly fills the input aperture. Fig. 5 shows the magnitude of the antisymmetric gradient force component, the symmetric scattering force component, and the total force, expressed as Q_g , Q_s , and Q_t , for values of S above and $(-S)$ below the center of the sphere. The sphere outline is shown in Fig. 5 for reference. It is seen that the trapping forces are largely confined within the spherical particle. The stable equilibrium point S_E of the trap is located just above the

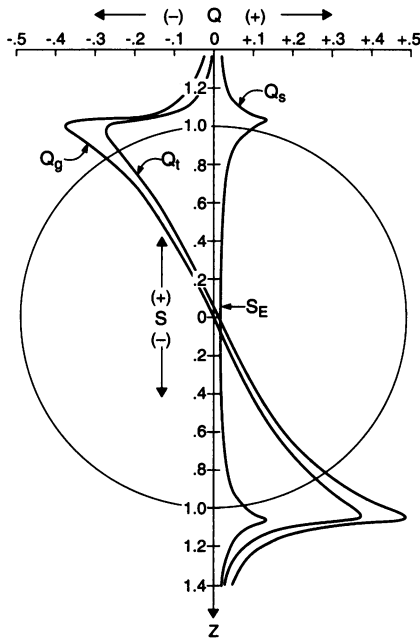


FIGURE 5 Values of the scattering force, gradient force, and total force Q_s , Q_g , and Q_t exerted on a sphere of index of refraction $n = 1.2$ by a trap with a uniformly filled input aperture which is focused along the Z axis at positions $+s$ above and $-s$ below the center of the sphere.

center of the sphere at $S \cong 0.06$, where the backward gradient force just balances the weak forward scattering force. Away from the equilibrium point the gradient force dominates over the scattering force and Q_t reaches its maximum value very close to the sphere edges at $S \cong 1.01$ and $(-S) \cong 1.02$. The large values of net restoring force near the sphere edges are due to the significant fraction of all incident rays which have both large values of θ , near the optimum value of 70° , and large convergence angle ϕ . This assures a large backward gradient force contribution from the component $F_g \sin \phi$ and also a much-reduced scattering force contribution from the component $F_s \cos \phi$.

Trap along Y axis

We next examine the trapping forces for the case where the focus f of the trapping beam is located transversely along the $-Y$ axis of the sphere as shown in Fig. 6. The details of the force computation are discussed in Appendix II. Fig. 7 plots the gradient force, scattering force, and total force in terms of Q_g , Q_s , and Q_t as a function of the distance S' of the trap focus from the origin along the $-Y$ axis for the same conditions as in III A. For this case the gradient force has only a $-Y$ component. The scattering force is orthogonal to it along the $+Z$ axis. The total force again maximizes at a value $Q_t \cong 0.31$ near the sphere edge at $S' \cong 0.98$ and makes a small angle $\phi = \arctan F_g/F_s \cong 18.5^\circ$ with respect to the Y axis. The Y force is, of course, symmetric about the center of the sphere at O .

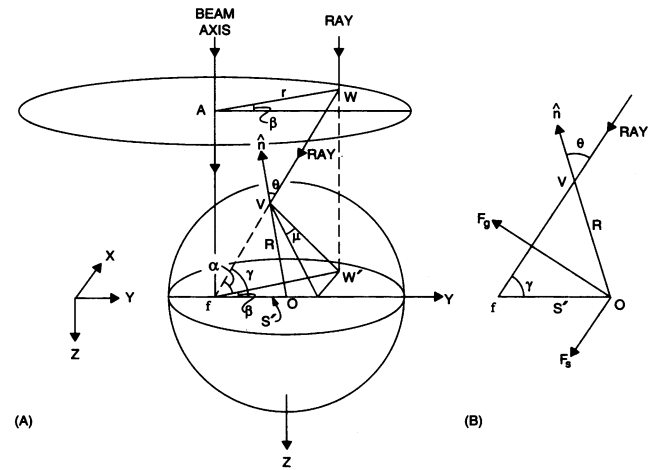


FIGURE 6 (A) Trap geometry with the beam focus f located transversely along the $-Y$ axis at a distance S' from the origin. (B) Geometry of the plane of incidence showing the directions of the gradient and scattering forces F_g and F_s for the input ray.

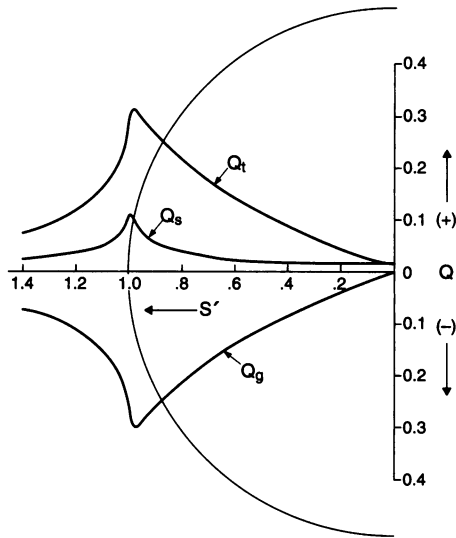


FIGURE 7 Plot of the gradient force, scattering force, and total force Q_g , Q_s , and Q_t as a function of the distance S' of trap focus from the origin along the $-Y$ axis for a circularly polarized trapping beam uniformly filling the aperture and a sphere of index of refraction $n = 1.2$.

General case: arbitrary trap location

Consider finally the most general case where the focus f is situated arbitrarily in the vertical plane through the Z axis at the distance S' from the sphere origin O in the direction of the $-Y$ axis and a distance S'' in the direction of the $-Z$ axis as shown in Fig. 8. Appendix III summarizes the method of force computation for this case.

Fig. 10 shows the magnitude and direction of the gradient force Q_g , the scattering force Q_s , and the total force Q_t as functions of the position of the focus f over the left half of the YZ plane, and by mirror image symmetry about the Y axis, over the entire cross-section of the sphere. This is again calculated for a circularly polarized beam uniformly filling the aperture and for $n = 1.2$. Although the force vectors are drawn at the point of focus f , it must be understood that the actual forces always act through the center of the sphere. This is true for all rays and therefore also for the full beam. It is an indication that no radiation pressure torques are possible on a sphere from the linear momentum of light. We see in Fig. 10A that the gradient force which is exactly radial along the Z and Y axes is also very closely radial (within an average of $\sim 2^\circ$ over the rest of the sphere. This stems from the closely radially uniform distribution of the incident light in the upper hemisphere. The considerably smaller scattering force is shown in Fig. 10B (note the change in scale). It is strictly

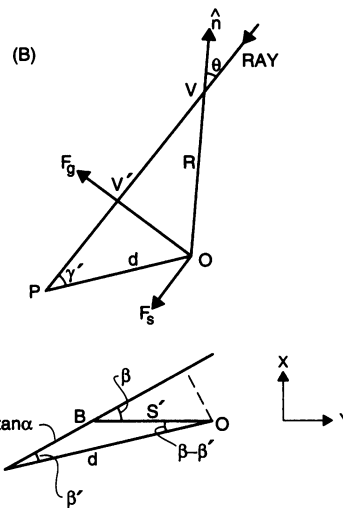
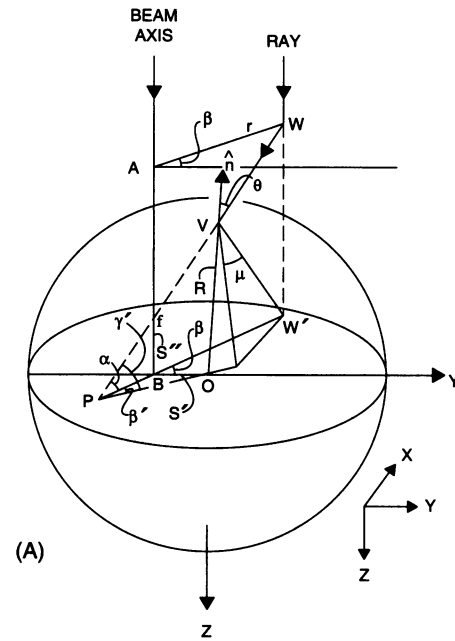


FIGURE 8 (A) Trap geometry with the beam focus located at a distance S' from the origin in the $-Y$ direction and a distance S'' in the $-Z$ direction. (B) Geometry of the plane of incidence POV showing the direction of gradient and scattering forces F_g and F_s for the ray. Geometry of triangle POB in the XY plane for finding β' and d .

axial only along the Z and Y axes and remains predominantly axial elsewhere except for the regions farthest from the Z and Y axes. It is the dominance of the gradient force over the scattering force that accounts for the overall radial character of the total force in Fig. 10C. The rapid changes in direction of the force that occur when the focus is well outside the sphere are mostly due to the rapid changes in effective beam direction as parts of the input beam start to miss the

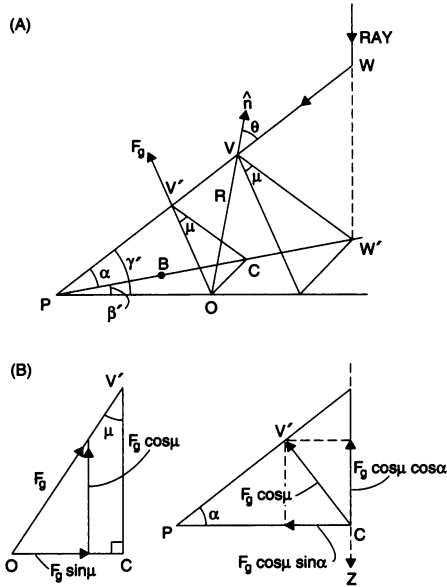


FIGURE 9 Another view of Fig. 8A containing the angle μ between the plane of incidence POV' and the vertical plane $WW'P$ for resolving force components along the coordinate axis.

sphere. We note that the magnitude of the total force Q_t maximizes very close to the edge of the sphere as we proceed radially outward in all directions, as does the gradient and scattering forces. The value of maximum restoring forces varies smoothly around the edge of the sphere from a minimum of $Q_t = 0.28$ in the axially backward direction to a maximum of $Q_t = 0.49$ in the forward direction. Thus, for these conditions the maximum trapping force achieved varies quite moderately over the sphere by a factor of $0.49/0.28 = 1.78$ and conforms closely to the edges of the sphere.

The line EE' marked on Fig. 10C represents the locus of points for which the Z component of the force is zero; i.e., the net force is purely horizontal. If one starts initially at point E, the equilibrium point of the trap with no externally applied forces, and then applies a +Y-directed Stokes force by flowing liquid past the sphere to the right, for example, the equilibrium position will shift to a new equilibrium point along EE' where the horizontal light force just balances the viscous force. With increasing viscous force the focus finally moves to E' , the point of maximum transverse force, after which the sphere escapes the trap. Notice that there is a net z displacement of the sphere as the equilibrium point moves from E to E' . We have observed this effect in experiments with micron-sized polystyrene spheres. Sato et al. (18) have recently reported also seeing this displacement.

EFFECT OF MODE PROFILES AND INDEX OF REFRACTION ON TRAPPING FORCES

To achieve a uniformly filled aperture in practice requires an input TEM_{00} mode Gaussian beam with very large spot size, which is wasteful of laser power. We therefore consider the behavior of the trap for other cases of TEM_{00} mode input beam profiles with smaller spot sizes, as well as TEM_{01} *‘‘do-nut’’ mode beam profiles which preferentially concentrate input light intensity at large input angles ϕ .

TEM_{00} mode profile

Table II compares the performance of traps with $n = 1.2$ having different TEM_{00} mode intensity profiles of the form $I(r) = I_0 \exp(-2r^2/w_0^2)$ at the input aperture of the microscope objective. The quantity a is the ratio of the TEM_{00} mode beam radius w_0 to the full lens aperture r_{max} . A is the fraction of total beam power that enters the lens aperture. A decreases as a increases. In the limit of a uniform input intensity distribution $A = 0$ and $a = \infty$. For $w_0 \leq r_{max}$ we define the convergence angle of the input beam as θ' where $\tan \theta' = w_0/\ell$. ℓ is the distance from the lens to the focus f as shown in Fig. 2B. For $w_0 > r_{max}$ the convergence angle is set by the full lens aperture and we use $\theta' = \phi_{max}$, where $\tan \phi_{max} = r_{max}/\ell$. For a NA = 1.25 water immersion objective $\phi_{max} = 70^\circ$. The quality of the trap can be characterized by the maximum strength of the restoring forces as one proceeds radially outward for the sphere origin O in three representative directions taken along the Z and Y axes. We thus list Q_{1max} , the value of the maximum restoring force along the $-Z$ axis, and S_{max} , the radial distance from the origin at which it occurs. Similarly listed are Q_{2max} occurring at S'_{max} along the $-Y$ axis and Q_{3max} occurring at $(-S)_{max}$ along the $+Z$ axis (see Figs. 2, 5, and 6 for a reminder on the definitions of S , $-S$, and S'). S_E in Table II gives the location of the equilibrium point of the trap along the $-Z$ axis as noted in Fig. 5.

One sees from Table II that the weakest of the three representative maximum restoring forces is Q_{1max} occurring in the $-Z$ direction. Furthermore, of all the traps the $a = \infty$ trap with a uniformly filled aperture has the largest Q_{1max} force and is therefore the strongest of all the TEM_{00} mode traps. One can also define the ‘‘escape force’’ of a given trap as the lowest force that can pull the particle free of the trap in any direction. In this context the $a = \infty$ trap has the largest magnitude of escape force of $Q_{1max} = 0.276$. One also sees that the $a = \infty$ trap is the most uniform trap since it has the smallest fractional variation in the extreme values of the restoring forces Q_{1max} and Q_{3max} . If, however, we reduce a to 1.7

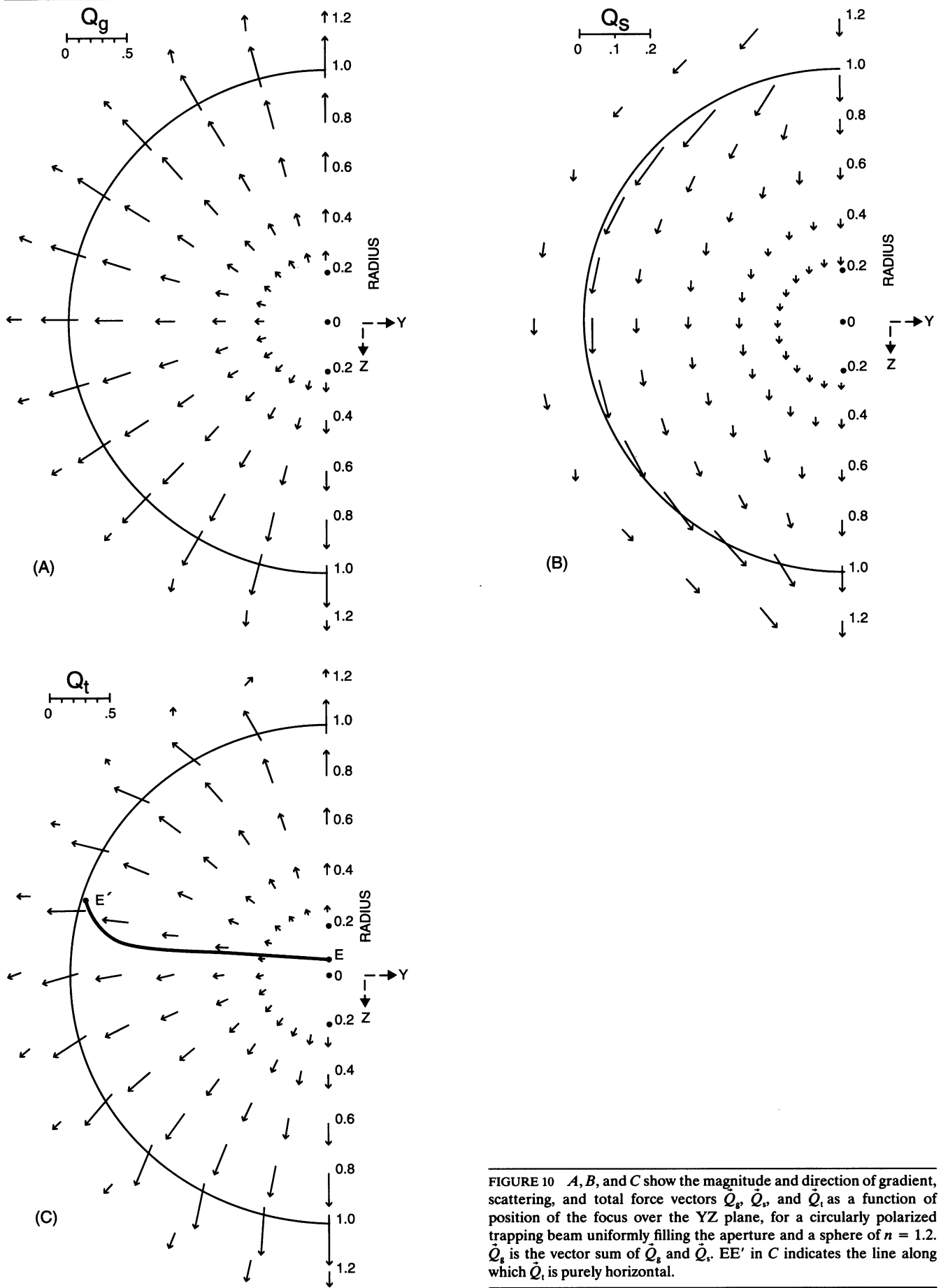


FIGURE 10 *A*, *B*, and *C* show the magnitude and direction of gradient, scattering, and total force vectors \vec{Q}_g , \vec{Q}_s , and \vec{Q}_t as a function of position of the focus over the *YZ* plane, for a circularly polarized trapping beam uniformly filling the aperture and a sphere of $n = 1.2$. \vec{Q}_t is the vector sum of \vec{Q}_g and \vec{Q}_s . *EE'* in *C* indicates the line along which \vec{Q}_t is purely horizontal.

TABLE 2 Performance of TEM₀ mode traps with $n = 1.2$ having different intensity profiles at the input of the microscope objective

| a | A | $[Q_{1\max}]$ | S_{\max} | $[Q_{2\max}]$ | S'_{\max} | $[Q_{3\max}]$ | $(-S)_{\max}$ | S_E | θ' |
|----------|------|---------------|------------|---------------|-------------|---------------|---------------|-------|-----------|
| ∞ | 0 | -0.276 | 1.01 | 0.313 | 0.98 | 0.490 | 1.05 | 0.06 | 70° |
| 1.7 | 0.5 | -0.259 | 1.01 | 0.326 | 0.98 | 0.464 | 1.05 | 0.08 | 70° |
| 1.0 | 0.87 | -0.225 | 1.02 | 0.349 | 0.98 | 0.412 | 1.05 | 0.10 | 70° |
| 0.727 | 0.98 | -0.184 | 1.03 | 0.383 | 0.98 | 0.350 | 1.06 | 0.13 | 63° |
| 0.364 | 1.0 | -0.077 | 1.15 | 0.498 | 0.98 | 0.214 | 1.3 | 0.32 | 45° |
| 0.202 | 1.0 | -0.019 | 1.4 | 0.604 | 0.98 | 0.147 | 1.9 | 0.80 | 29° |

or even 1.0, where the fraction of input power entering the aperture is reasonably high (~ 0.50 or 0.87), one can still get performance close to that of the uniformly filled aperture. Trap performance, however, rapidly degrades for cases of underfilled input aperture and decreasing beam convergence angle. For example, in the trap with $a = 0.202$ and $\theta' \cong 29^\circ$ the value of $Q_{1\max}$ has dropped more than an order of magnitude to $Q_{1\max} = -0.019$. The maximum restoring forces $Q_{1\max}$ and $Q_{2\max}$ occur well outside the sphere and the equilibrium position has moved away from the origin to $S_E = 0.8$. This trap with $\theta' \cong 29^\circ$ roughly corresponds to the best of the traps described by Wright et al. (27) (for the case of $w_0 = 0.5 \mu\text{m}$). They find for $w_0 = 0.5 \mu\text{m}$ that the trap has an equilibrium position outside of the sphere and a maximum trapping force equivalent to $Q_{1\max} = -0.055$. Any more direct comparison of our results with those of Wright et al. is not possible since they use an approximate force calculation which overestimates the forces somewhat. They do not calculate forces for the beam focus inside the sphere and there are other artifacts associated with their use of Gaussian beam phase fronts to give the incident ray directions near the beam focus.

TEM₀₁* “do-nut” mode profile

Table III compares the performance of several traps based on the TEM₀₁* mode, the so-called “do-nut” mode, which has an intensity distribution of the form $I(r) = I_0 (r/w_0')^2 \exp(-2r^2/w_0'^2)$. The quantity a is now the ratio

of w_0' , the spot size of the do-nut mode, to the full lens aperture r_{\max} . All other items in the table are the same as in Table II. For $a = 0.76 \sim 87\%$ of the total beam power enters the input aperture r_{\max} and one obtains performance that is almost identical to that of the trap with uniformly filled aperture as listed in Table II. For larger values of a the absolute magnitude of $Q_{1\max}$ increases, the magnitude of $Q_{2\max}$ decreases, and the fraction of power entering the aperture decreases. Optimal trapping, corresponding to the highest value of escape force, is achieved at values of $a \cong 1.0$ where the magnitudes $Q_{1\max} \cong Q_{2\max} \cong 0.30$. This performance is somewhat better than achieved with TEM₀₀ mode traps.

It is informative to compare the performance of do-nut mode traps with that of a so-called “ring trap” having all its power concentrated in a ring 95–100% of the full beam aperture, for which $\phi \cong \phi_{\max} = 70^\circ$. When the ring trap is focused at $S \cong 1.0$ essentially all of the rays hit the sphere at an angle of incidence very close to $\theta_{g\max} = 72^\circ$, the angle that makes Q_g a maximum for $n = 1.2$ (see Table I). Thus the resulting backward total force of $Q_{1\max} = 0.366$ at $S = 0.99$, as listed in Table III, closely represents the highest possible backward force on a sphere of $n = 1.2$. The ring trap, however, has a reduced force $Q_{2\max} = 0.254$ at $S'_{\max} = 0.95$ in the $-Y$ direction since many rays at this point are far from optimal. If we imagine adding an axial beam to the ring beam then we optimally increase the gradient contribution to the force in the $-Y$ direction near $S' = 1.0$ and decrease the

TABLE 3 Performance of TEM₀₁* mode traps with $n = 1.2$ having different intensity profiles at the input of the microscope objective

| a | A | $[Q_{1\max}]$ | S_{\max} | $[Q_{2\max}]$ | S'_{\max} | $[Q_{3\max}]$ | $(-S)_{\max}$ | S_E |
|---------------------------------------|------|---------------|------------|---------------|-------------|---------------|---------------|-------|
| TEM ₀₁ * do-nut mode traps | | | | | | | | |
| 1.21 | 0.40 | -0.310 | 1.0 | 0.290 | 0.98 | 0.544 | 1.05 | 0.06 |
| 1.0 | 0.59 | -0.300 | 1.01 | 0.296 | 0.98 | 0.531 | 1.05 | 0.06 |
| 0.938 | 0.66 | -0.296 | 1.01 | 0.298 | 0.98 | 0.525 | 1.05 | 0.07 |
| 0.756 | 0.87 | -0.275 | 1.01 | 0.311 | 0.98 | 0.494 | 1.06 | 0.10 |
| Ring beam with $\phi = 70^\circ$ | | | | | | | | |
| | | -0.366 | 0.99 | 0.254 | 0.95 | 0.601 | 1.03 | |
| Ring beam plus axial beam | | | | | | | | |
| | | -0.31 | 0.99 | 0.31 | 0.95 | 0.51 | 1.03 | |

Comparison data on a Ring Beam having $\phi = 70^\circ$ and a Ring Beam plus an Axial Beam containing 18% of the power.

overall force in the $-Z$ direction. With 18% of the power in the axial beam one gets $Q_{1\max} = Q_{2\max} \cong 0.31$. This performance is now close to that of the optimal do-nut mode trap. It is possible to design gradient traps that approximate the performance of a ring trap using a finite number of individual beams (for example, four, three or two beams) located symmetrically about the circumference of the ring and converging to a common focal point at angles of $\phi \cong 70^\circ$. Recent reports (32, 33) at the CLEO-'91 conference presented observations on a trap with two individual beams converging to a focus with $\phi \cong 65^\circ$ and also on a single beam gradient trap using the TEM₀₁* mode.

Knowledge of the forces produced by ring beams allows one to compare the forces generated by bright field microscope objectives, as have thus far been considered, with the forces from phase contrast objectives of the same NA. For example, assume a phase contrast objective having an 80% absorbing phase ring located between radii of 0.35 and 0.55 of the full input lens aperture. For the case of an input beam uniformly filling the aperture with $n = 1.2$, one finds that the bright field escape force of $Q_{1\max} = 0.276$ (see Table II) increases by $\sim 4\%$ to $Q_{1\max} = 0.287$ in going to the phase contrast objective. With a TEM₀₀ mode Gaussian beam input having $A = 0.87$ and $n = 1.2$, the bright field escape force magnitude of $Q_{1\max} = 0.225$ increases by $\sim 2\%$ to $Q_{1\max} = 0.230$ for a phase contrast objective. The reason for these slight improvements is that the force contribution of rays at the ring corresponds to $Q_{1\max} \cong 0.204$, which is less than the average force for bright field. Thus any removal of power at the ring radius improves the overall force per unit transmitted power. Differential interference contrast optics can make use of the full

input lens aperture and thus gives equivalent trapping forces to bright field optics.

Index of refraction effects

Consider, finally, the role of the effective index of refraction of the particle $n = n_1/n_2$ on the forces of a single-beam gradient trap. In Table IV we vary n for two types of trap, one with a uniformly filled input aperture, and the other having a do-nut input beam with $a = 1.0$, for which the fraction of total power feeding the input aperture is 59%. For the case of the uniformly filled aperture we get good performance over the range $n = 1.05$ to $n \cong 1.5$, which covers the regime of interest for most biological samples. At higher index $Q_{1\max}$ falls to a value of -0.097 at $n = 2$. This poorer performance is due to the increasing scattering force relative to the maximum gradient force as n increases (see Table I). Also the angle of incidence for maximum gradient force falls for higher n . At $n = 2$ (which corresponds roughly to a particle of index ~ 2.7 in water of index 1.33), the do-nut mode trap is clearly better than the uniform beam trap.

CONCLUDING REMARKS

It has been shown how to define the gradient and scattering forces acting on dielectric spheres in the ray optics regime for beams of complex shape. One can then describe the operation of single beam gradient force traps for spheres of diameter $\gg \lambda$ in terms of the dominance of an essentially radial gradient force over the predominantly axial scattering force. This is analogous to the previous description of the operation of this

TABLE 4 Effect of index of refraction n on the performance of a trap with a uniformly filled aperture ($a = \infty$) and a do-nut trap with $a = 1.0$

| n | $[Q_{1\max}]$ | S_{\max} | $[Q_{2\max}]$ | S'_{\max} | $[Q_{3\max}]$ | $(-S)_{\max}$ | S_E |
|---|---------------|------------|---------------|-------------|---------------|---------------|-------|
| Trap with uniformly filled aperture | | | | | | | |
| 1.05 | -0.171 | 1.06 | 0.137 | 1.00 | 0.219 | 1.06 | 0.02 |
| 1.1 | -0.231 | 1.05 | 0.221 | 0.99 | 0.347 | 1.06 | 0.04 |
| 1.2 | -0.276 | 1.01 | 0.313 | 0.98 | 0.490 | 1.05 | 0.06 |
| 1.3 | -0.288 | 0.96 | 0.368 | 0.97 | 0.573 | 1.04 | 0.11 |
| 1.4 | -0.282 | 0.93 | 0.403 | 0.96 | 0.628 | 1.02 | 0.15 |
| 1.6 | -0.237 | 0.89 | 0.443 | 0.94 | 0.693 | 1.00 | 0.25 |
| 1.8 | -0.171 | 0.88 | 0.461 | 0.94 | 0.723 | 0.99 | 0.37 |
| 2.0 | -0.097 | 0.88 | 0.469 | 0.94 | 0.733 | 0.99 | 0.53 |
| TEM ₀₁ * do-nut mode trap with $a = 1.0$ | | | | | | | |
| 1.05 | -0.185 | 1.06 | 0.134 | 1.00 | 0.238 | 1.06 | 0.02 |
| 1.1 | -0.250 | 1.05 | 0.208 | 0.99 | 0.379 | 1.06 | 0.03 |
| 1.2 | -0.300 | 1.01 | 0.296 | 0.98 | 0.531 | 1.05 | 0.06 |
| 1.4 | -0.309 | 0.93 | 0.382 | 0.95 | 0.667 | 1.02 | 0.13 |
| 1.8 | -0.204 | 0.88 | 0.434 | 0.94 | 0.748 | 0.99 | 0.32 |
| 2.0 | -0.132 | 0.88 | 0.439 | 0.94 | 0.752 | 0.99 | 0.42 |

trap in the Rayleigh regime, where the diameter $\ll \lambda$. Quite strong uniform traps are possible for $n = 1.2$ using the TEM_{01}^* do-nut mode in which the trapping forces vary over the sphere cross-section from a Q value of -0.30 in the $-Z$ direction to 0.53 in the $+Z$ direction. The magnitude of trapping force of 0.30 in the weakest trapping direction gives the escape force which a spherically shaped motile living organism, for example, must exert in order to escape the trap. For a laser power of 10 mW the minimum trapping force or escape force of $Q = 0.30$ is equivalent to 1.2×10^{-6} dynes. This implies that a motile organism $10 \mu\text{m}$ in diameter which is capable of propelling itself through water at a speed of $128 \mu\text{m/s}$ will be just able to escape the trap in its weakest direction along the $-Z$ axis. The only possible drawback to using the do-nut mode in practice is the difficulty of generating that mode in the laser. With the simpler TEM_{00} mode beams one can achieve traps with Q 's as high as 0.23 , for example, with 87% of the laser power entering the aperture of the microscope objective.

The calculation confirms the importance of using beams with large convergence angles θ' as high as $\sim 70^\circ$ for achieving strong traps, especially with particles having lower indices of refraction typical of biological samples. At small convergence angles, less than $\sim 30^\circ$, the scattering force dominates over the gradient force and single beam trapping is either marginal or not possible. One can, however, make a two-beam gradient force trap using smaller convergence angles based on two confocal, oppositely directed beams of equal power in which each ray of the converging beam is exactly matched by an oppositely directed ray. Then the scattering forces cancel and the gradient forces add, giving quite a good trap. Gradient traps of this type have been previously observed in experiments on alternating beam traps (34). The advantage of lower beam convergence is the ability to use longer working distances.

This work using ray optics extends the quantitative description of the single beam gradient trap for spheres to the size regime where the diameter is $\gg \lambda$. In this regime the force is independent of particle radius r . In the Rayleigh regime the force varies as r^3 . At present there is no quantitative calculation for the intermediate size regime where the diameter is $\approx \lambda$, in which we expect force variations between r^0 and r^3 . This is a more difficult scattering problem and involves an extension of Mie theory (35) or vector methods (36) to the case of highly convergent beams. Experimentally, however, this intermediate regime presents no problems. One can often directly calibrate the magnitude of the trapping force using Stokes dragging forces and thus successfully perform experiments with biological particles of size $\approx \lambda$ (16).

One can get a good idea of the range of validity of the

trapping forces as computed in the ray optics regime from a comparison of the scattering of a plane wave by a large dielectric sphere in the ray optics regime with the exact scattering, including all diffraction effects, as given by Mie theory. It suffices to consider plane waves since complex beams can be decomposed into a sum of plane waves. It was shown by van de Hulst in Chapter 12 of his book (35) that ray optics gives a reasonable approximation to the exact angular intensity distribution of Mie theory (except in a few special directions) for sphere size parameters $2\pi r/\lambda = 10$ or 20 . The special directions are the forward direction, where a large diffraction peak appears which contributes nothing to the radiation pressure, and the so-called glory and rainbow directions, where ray optics never works. Since these directions contribute only slightly to the total force, we expect ray optics to give fair results down to diameters of approximately six wavelengths or $\sim 5 \mu\text{m}$ for a $1.06\text{-}\mu\text{m}$ laser beam in water. The validity of the approximation should improve rapidly at larger sphere diameters. A similar result was also derived by van de Hulst (35) using Fresnel zones to estimate diffractive effects.

One of the advantages of a reliable theoretical value for the trapping force is that it can serve as a reference for comparison with experiment. If discrepancies appear in such a comparison one can then look for the presence of other forces. For traps using infrared beams there could be significant thermal (radiometric) force contributions due to absorptive heating of the particle or surrounding medium whose magnitude could then be inferred. Detailed knowledge of the variation of trapping force with position within the sphere is also proving useful in measurements of the force of swimming sperm (15).

Received for publication 19 June 1991 and in final form 16 August 1991.

APPENDIX I

Force of a ray on a dielectric sphere

A ray of power P hits a sphere at an angle θ where it partially reflects and partially refracts, giving rise to a series of scattered rays of power $PR, PT^2, PT^2R, \dots, PT^2R^n, \dots$. As seen in Fig. 3, these scattered rays make angles relative to the incident forward ray direction of $\pi + 2\theta, \alpha, \alpha + \beta, \dots, \alpha + n\beta, \dots$, respectively. The total force in the Z direction is the net change in momentum per second in the Z direction due to the scattered rays. Thus:

$$F_z = \frac{n_1 P}{c} - \left[\frac{n_1 PR}{c} \cos(\pi + 2\theta) + \sum_{n=0}^{\infty} \frac{n_1 P}{c} T^2 R^n \cos(\alpha + n\beta) \right], \quad (\text{A1})$$

where $n_1 P/c$ is the incident momentum per second in the Z direction. Similarly for the Y direction, where the incident momentum per second is zero, one has:

$$F_Y = 0 - \left[\frac{n_1 P R}{c} \sin(\pi + 2\theta) - \sum_{n=0}^{\infty} \frac{n_1 P}{c} T^2 R^n \sin(\alpha + \beta) \right]. \quad (\text{A2})$$

As pointed out by van de Hulst in Chapter 12 of reference 35 and by Roosen (22), one can sum over the rays scattered by a sphere by considering the total force in the complex plane, $F_{\text{tot}} = F_Z + iF_Y$. Thus:

$$F_{\text{tot}} = \frac{n_1 P}{c} [1 + R \cos 2\theta] + i \frac{n_1 P}{c} R \sin 2\theta - \frac{n_1 P}{c} T^2 \sum_{n=0}^{\infty} R^n e^{i(\alpha+n\beta)}. \quad (\text{A3})$$

The sum over n is a simple geometric series which can be summed to give:

$$F_{\text{tot}} = \frac{n_1 P}{c} [1 + R \cos 2\theta] + i \frac{n_1 P}{c} R \sin 2\theta - \frac{n_1 P}{c} T^2 e^{i\alpha} \left[\frac{1}{1 - R e^{i\beta}} \right]. \quad (\text{A4})$$

If one rationalizes the complex denominator and takes the real and imaginary parts of F_{tot} , one gets the force expressions A1 and A2 for F_Z and F_Y using the geometric relations $\alpha = 2\theta - 2r$ and $\beta = \pi - 2r$, where θ and r are the angles of incidence and refraction of the ray.

APPENDIX II

Force on a sphere for trap focus along Y axis

We treat the case of the beam focus located along the $-Y$ axis at a distance S' from the origin O (see Fig. 6). We first calculate the angle of incidence θ for an arbitrary ray entering the input lens aperture vertically at a radius r and azimuthal angle β in the first quadrant. On leaving the lens the ray stays in the vertical plane AWW' and heads in the direction towards f , striking the sphere at V . The forward projection of the ray makes an angle α with respect to the horizontal (X, Y) plane. The plane of incidence, containing both the input ray and the normal to the sphere OV , is the so-called γ plane fOV which meets the horizontal and vertical planes at f . Knowing α and β , we find γ from the geometrical relation $\cos \gamma = \cos \alpha \cos \beta$. Referring to the γ plane we can now find the angle of incidence θ from $R \sin \theta = S' \sin \gamma$ putting $R = 1$.

In contrast to the focus along the Z axis, the net force now depends on the choice of input polarization. For the case of an incident beam polarized perpendicular to the Y axis, for example, one first resolves the polarized electric field E into components $E \cos \beta$ and $E \sin \beta$ perpendicular and parallel to the vertical plane containing the ray. Each of these components can be further resolved into the so-called p and s components parallel and perpendicular to the plane of incidence in terms of these angle μ between the vertical plane and the plane of incidence. By geometry, $\cos \mu = \tan \alpha / \tan \gamma$. This resolution yields fractions of the input power in the p and s components given by:

$$f_p = (\cos \beta \sin \mu - \sin \beta \cos \mu)^2 \quad (\text{A5})$$

$$f_s = (\cos \beta \cos \mu + \sin \beta \sin \mu)^2. \quad (\text{A6})$$

If the incident polarization is parallel to the Y axis, then f_p and f_s reverse. Knowing θ, f_p , and f_s , one computes the gradient and scattering force components for p and s separately using Eqs. A5 and A6 and adds the results.

The net gradient and scattering force contribution of the ray thus computed must now be resolved into components along the coordinate axes (see Fig. 6 B). However, comparing the force contributions of the quartet of rays made up of the ray in the first quadrant and its mirror image rays in the other quadrants we see that the magnitudes of the forces are identical for each of the rays of the quartet. Furthermore, the scattering and gradient forces of the quartet are directly symmetrically about the Z and Y axes, respectively. This symmetry implies that the entire beam can only give rise to a net Z scattering force coming from the integral of the $F_i \cos \phi$ component and a net Y gradient force coming from the $F_i \sin \gamma$ component. In practice we need only integrate these components over the first quadrant and multiply the results by 4 to get the net force. The differences in force that result from the choice of input polarization perpendicular or parallel to the Y axis are not large. For the conditions of Fig. 7 the maximum force difference is $\sim 14\%$ near $S' \cong 1.0$. We have therefore made calculations using a circularly polarized input beam with $f_p = f_s = 1/2$, which yields values of net force that are close to the average of the forces for the two orthogonally polarized beams.

APPENDIX III

Force on a sphere for an arbitrarily located trap focus

We now treat the case where the trapping beam is focused arbitrarily in the XY plane at a point f located at a distance S' from the origin in the $-Y$ direction and a distance S'' in the $-Z$ direction (see Fig. 8). To calculate the force for a given ray we again need to find the angle of incidence θ and the fraction of the ray's power incident on the sphere in the s and p polarizations. Consider a ray of the incident beam entering the input aperture of the lens vertically at a radius r and azimuthal angle β in the first quadrant. The ray on leaving the lens stays in the vertical plane $AWW'B$ and heads toward f , hitting the sphere at V . The extension of the incident ray to f and beyond intersects the XY plane at point P at an angle α . The plane of incidence for this ray is the so-called γ' plane POV which contains both the incident ray and the normal to the sphere OV . Referring to the planar figure in Fig. 8 B one can find the angle β' by simple geometry in terms of S', S'' , and the known angles α and β from the relation

$$\tan \beta' = \frac{S' \sin \beta}{S' \cos \beta + S'' / \tan \alpha}. \quad (\text{A7})$$

We get γ' from $\cos \gamma' = \cos \alpha \cos \beta'$. Referring to the γ' plane in Fig. 8 B we get the angle of incidence θ for the ray from $R \sin \theta = d \sin \gamma'$, putting $R = 1$. The distance d is deduced from the geometric relation:

$$d = \frac{S'' \cos \beta'}{\tan \alpha} + S' \cos(\beta - \beta'). \quad (\text{A8})$$

As in Appendix II, we compute f_p and f_s , the fraction of the ray's power in the p and s polarizations, in terms of the angle μ between the vertical plane $W'VP$ and the plane of incidence POV . We use Eqs. A5 and A6 for the case of a ray polarized perpendicular to the Y axis and

the same expressions with f_p and f_s reversed for a ray polarized parallel to the Y axis. To find μ we use $\cos \mu = \tan \alpha / \tan \gamma'$. As in Appendix II we can put $f_p = f_s = 1/2$ and get the force for a circularly polarized ray, which is the average of the force for the cases of two orthogonally polarized rays.

The geometry for resolving the net gradient and scattering force contribution of each ray of the beam into components along the axes is now more complex. The scattering force F_s is directed parallel to the incident ray in the VP direction of Fig. 8. It has components $F_s \sin \alpha$ in the +Z direction and $F_s \cos \alpha$ pointing in the BP direction in the XY plane. $F_s \cos \alpha$ is then resolved with the help of Fig. 8B into $F_s \cos \alpha \cos \beta$ in the -Y direction and $F_s \cos \alpha \sin \beta$ in the -X direction. The gradient force F_g points in the direction OV' perpendicular to the incident ray direction VP in the plane of incidence OPV. This is shown in Fig. 8 and also Fig. 9, which gives yet another view of the geometry. In Fig. 9 we consider the plane V'OC, which is taken perpendicular to the γ' plane POV and the vertical plane WW'P. This defines the angle OV'C as μ , the angle between the planes, and also makes the angles OCV', OCP, and CV'P right angles. As an aid to visualization one can construct a true three-dimensional model out of cardboard of the geometric figure for the general case as shown in Figs. 8 and 9. Such a model will make it easy to verify that the above stated angles are indeed right angles, and to see other details of the geometry. We can now resolve F_g into components along the X, Y, and Z axes with the help of right triangles OV'C and CV'P as shown in Fig. 9B. In summary, the net contribution of a ray in the first quadrant to the force is:

$$F(Z) = F_s \sin \alpha + F_g \cos \mu \cos \alpha \quad (\text{A9})$$

$$F(Y) = -F_s \cos \alpha \cos \beta + F_g \cos \mu \sin \alpha \cos \beta + F_g \sin \mu \sin \beta \quad (\text{A10})$$

$$F(X) = -F_s \cos \alpha \sin \beta + F_g \cos \mu \sin \alpha \sin \beta - F_g \sin \mu \cos \beta. \quad (\text{A11})$$

The force equations A9–A11 are seen to have the correct signs since F_s and F_g are, respectively, positive and negative as calculated from Eqs. 1 and 2.

For the general case under consideration we lose all symmetry between first and second quadrant forces and we must extend the force integrals into the second quadrant. All the above formulas which were derived for rays of the first quadrant are equally correct in the second quadrant using the appropriate values of the angles β , β' , γ' , and μ . For example, in the second quadrant β' can be obtuse. This gives obtuse γ' and obtuse μ . Obtuse μ implies that the γ' plane has rotated its position beyond the perpendicular to the vertical plane AWW'. In this orientation the gradient force direction tips below the XY plane and reverses its Z component as indicated by the sign change in the $F_g \cos \mu \cos \alpha$ term.

There are, however, some symmetry relations in the force contributions of rays of the input beam which still apply. For example, there is symmetry about the Y axis; i.e., rays of the third and fourth quadrants give the same contribution to the Z and Y forces as rays of the first and second quadrants, whereas their X contributions exactly cancel. To find the net force we need only integrate the Y and Z components of first and second quadrants and double the result.

If we make S'' negative in all formulas, we obtain the correct magnitudes and directions of the forces for the case of the focus below the XY plane. Although we find different total force values for S'' positive and S'' negative, i.e., symmetrical beam focus points above and below the XY plane, there still are symmetry relations that apply to the scattering and gradient forces separately. Thus we find that the

Z components of the scattering force are the same above and below but the Y component reverse. For the gradient force the Z components reverse above and below and the Y components are the same. This is seen to be true in Fig. 10. It is also consistent with Fig. 5 showing the forces along the Z axis. This type of symmetry behavior arises from the fact that the angle of incidence for rays entering the first quadrant from above the XY plane (S'' positive) is the same as for symmetrical rays entering in the second quadrant below the XY plane (S'' negative). Likewise the angles of incidence are the same for the second quadrant above and the first quadrant below. These results permit one to directly deduce the force below the XY plane from the values computed above the XY plane. The results derived here for the focus placed at an arbitrary point within the YZ plane are perfectly general since one can always choose to calculate the force in the cross-sectional plane through the Z axis that contains the focus f .

As a check on the calculations one can show that the results putting $S'' = 0$ in the general case are identical with those from the simpler Y axis integrals derived in Appendix II. Also in the limit $S' \rightarrow 0$ one gets the same results as are given by the simpler Z axis integral discussed above.

REFERENCES

1. Ashkin, A. 1970. Acceleration and trapping of particles by radiation pressure. *Phys. Rev. Lett.* 24:156–159.
2. Ashkin, A. 1970. Atomic-beam deflection by resonance-radiation pressure. *Phys. Rev. Lett.* 24:1321–1324.
3. Roosen, G. 1979. Optical levitation of spheres. *Can. J. Phys.* 57:1260–1279.
4. Ashkin, A. 1980. Applications of laser radiation pressure. *Science (Wash. DC)* 210:1081–1088.
5. Chu, S., J. E. Bjorkholm, A. Ashkin, and A. Cable. 1986. Experimental observation of optically trapped atoms. *Phys. Rev. Lett.* 57:314–317.
6. Chu, S., and C. Wieman. 1989. Feature editors, special edition, laser cooling and trapping of atoms. *J. Opt. Soc. Am.* B6:2020–2278.
7. Misawa, H., M. Koshioka, K. Sasaki, N. Kitamura, and H. Masuhara. 1990. Laser trapping, spectroscopy, and ablation of a single latex particle in water. *Chem. Lett.* 8:1479–1482.
8. Ashkin, A., and J. M. Dziedzic. 1987. Optical trapping and manipulation of viruses and bacteria. *Science (Wash. DC)* 235:1517–1520.
9. Buican, T., M. J. Smith, H. A. Crissman, G. C. Salzman, C. C. Stewart, and J. C. Martin. 1987. Automated single-cell manipulation and sorting by light trapping. *Appl. Opt.* 26:5311–5316.
10. Ashkin, A., J. M. Dziedzic, and T. Yamane. 1987. Optical trapping and manipulation of single cells using infrared laser beams. *Nature (Lond.)* 330:769–771.
11. Block, S. M., D. F. Blair, and H. C. Berg. 1989. Compliance of bacterial flagella measured with optical tweezers. *Nature (Lond.)* 338:514–518.
12. Berns, M. W., W. H. Wright, B. J. Tromberg, G. A. Profeta, J. J. Andrews, and R. J. Walter. 1989. Use of a laser-induced force trap to study chromosome movement on the mitotic spindle. *Proc. Natl. Acad. Sci. USA.* 86:4539–4543.
13. Ashkin, A., and J. M. Dziedzic. 1989. Internal cell manipulation using infrared laser traps. *Proc. Natl. Acad. Sci. USA.* 86:7914–7918.
14. Tadir, Y., W. H. Wright, O. Vafa, T. Ord, R. H. Asch, and M. W.

-
- Berns. 1989. Micromanipulation of sperm by a laser generated optical trap. *Fertil Steril.* 52:870–873.
15. Bonder, E. M., J. Colon, J. M. Dziedzic, and A. Ashkin. 1990. Force production by swimming sperm-analysis using optical tweezers. *J. Cell Biol.* 111:421A.
16. Ashkin, A., K. Schütze, J. M. Dziedzic, U. Euteneuer, and M. Schliwa. 1990. Force generation of organelle transport measured in vivo by an infrared laser trap. *Nature (Lond.)*. 348:346–352.
17. Block, S. M., L. S. B. Goldstein, and B. J. Schnapp. 1990. Bead movement by single kinesin molecules studied with optical tweezers. *Nature (Lond.)*. 348:348–352.
18. Sato, S., M. Ohyumi, H. Shibata, and H. Inaba. 1991. Optical trapping of small particles using 1.3 μm compact InGaAsP diode laser. *Optics Lett.* 16:282–284.
19. Gordon, J. P. 1973. Radiation forces and momenta in dielectric media. *Phys. Rev. A.* 8:14–21.
20. Ashkin, A. 1978. Trapping of atoms by resonance radiation pressure. *Phys. Rev Lett.* 40:729–732.
21. Gordon, J. P., and A. Ashkin. 1980. Motion of atoms in a radiation trap. *Phys. Rev. A.* 21:1606–1617.
22. Roosen, G., and C. Imbert. 1976. Optical levitation by means of 2 horizontal laser beams—theoretical and experimental study. *Physics. Lett.* 59A:6–8.
23. Ashkin, A., and J. M. Dziedzic. 1971. Optical levitation by radiation pressure. *Appl. Phys. Lett.* 19:283–285.
24. Ashkin, A., and J. M. Dziedzic. 1975. Optical levitation of liquid drops by radiation pressure. *Science (Wash. DC)*. 187:1073–1075.
25. Ashkin, A., J. M. Dziedzic, J. E. Bjorkholm and S. Chu. 1986. Observation of a single-beam gradient force optical trap for dielectric particles. *Optics Lett.* 11:288–290.
26. Ashkin, A., and J. M. Dziedzic. 1989. Optical trapping and manipulation of single living cells using infra-red laser beams. *Ber. Bunsen-Ges. Phys. Chem.* 98:254–260.
27. Wright, W. H., G. J. Sonek, Y. Tadir, and M. W. Berns. 1990. Laser trapping in cell biology. *IEEE (Inst. Electr. Electron. Eng.) J. Quant. Elect.* 26:2148–2157.
28. Born, M., and E. Wolf. 1975. Principles of Optics. 5th ed. Pergamon Press, Oxford. 109–132.
29. Mansfield, S. M., and G. Kino. 1990. Solid immersion microscope. *Appl. Phys. Lett.* 57:2615–2616.
30. Richards, B., and E. Wolf. 1959. Electromagnetic diffraction in optical systems. II. Structure of the image field in an aplanatic system. *Proc. R. Soc. London. A.* 253:358–379.
31. Ashkin, A., and J. M. Dziedzic. 1973. Radiation pressure on a free liquid surface. *Phys. Rev. Lett.* 30:139–142.
32. Hori, M., S. Sato, S. Yamaguchi, and H. Inaba. 1991. Two-crossing laser beam trapping of dielectric particles using compact laser diodes. Conference on Lasers and Electro-Optics, 1991 (Optical Society of America, Washington, D.C.). *Technical Digest.* 10:280–282.
33. Sato, S., M. Ishigure, and H. Inaba. 1991. Application of higher-order-mode Nd:YAG laser beam for manipulation and rotation of biological cells. Conference on Lasers and Electro-Optics, 1991 (Optical Society of America, Washington, D.C.). *Technical Digest.* 10:280–281.
34. Ashkin, A., and J. M. Dziedzic. 1985. Observation of radiation pressure trapping of particles using alternating light beams. *Phys. Rev. Lett.* 54:1245–1248.
35. van de Hulst, H. C. 1981. Light Scattering by Small Particles. Dover Press, New York. 114–227.
36. Kim, J. S., and S. S. Lee. 1983. Scattering of laser beams and the optical potential well for a homogeneous sphere. *J. Opt. Soc. Am.* 73:303–312.